Perspective

Nonlinear chiral metaphotonics: a perspective

Kirill Koshelev,[a,*,†] **Pavel Tonkaev**[a,†] **and Yuri Kivshar**[a,*]
[a]Australian National University, Research School of Physics, Nonlinear Physics Center, Canberra, Australian Capital Territory, Australia

Abstract. We review the physics and some applications of photonic structures designed for the realization of strong nonlinear chiroptical response. We pay much attention to the recent strategy of utilizing different types of optical resonances in metallic and dielectric subwavelength structures and metasurfaces, including surface plasmon resonances, Mie resonances, lattice-guided modes, and bound states in the continuum. We summarize earlier results and discuss more recent developments for achieving large circular dichroism combined with the high efficiency of nonlinear harmonic generation.

1 Introduction

The chirality of an object is defined by complete absence of its mirror symmetries. With this property, chiral structures can be divided into two groups of enantiomers representing mirror images of each other. Natural chirality is associated with a microscopic material structure of chiral ions and molecules. The degree of chirality can be probed by circularly polarized light, which allows for distinguishing enantiomers via chiroptical effects arising due to different interaction of light with left and right polarizations and media.[1] In practice, electromagnetic waves with circular polarization are widely employed in a variety of applications in photonics, biology, and chemistry, including ultrafast magnetic imaging[2] and spectroscopy.[3]

Chiroptical effects manifesting optical activity can be expressed in terms of optical rotatory dispersion (ORD), in which the wave polarization plane is rotated after propagation through a chiral medium, and circular dichroism (CD),[4] which describes asymmetric transmission or absorption of circularly polarized light inside a chiral medium. The CD can be evaluated as $(I_{\text{RCP}}^{(\omega)} - I_{\text{LCP}}^{(\omega)})/(I_{\text{RCP}}^{(\omega)} + I_{\text{LCP}}^{(\omega)})$, where $I_{\text{RCP(LCP)}}^{(\omega)}$ is the co-polarized transmitted or absorbed power for RCP (LCP) excitation and selective RCP (LCP) collection. In natural materials, optical activity is very weak. Over the last two decades, artificial materials with chirality engineered at the macroscopic level have been introduced to enhance weak natural chiroptical effects. In earlier studies, three-dimensional (3D) chiral metamaterials were shown to enhance ORD and CD in the linear regime and provide a simpler route to negative refraction.[5–7] Due to the complexity of experimental realization of bulk chiral metamaterials, the research focus shifted toward the study of planar chiral structures composed of ordered arrays of subwavelength scatterers, which were demonstrated to change the polarization state of light in a way similar to 3D chiral media.[8–11]

Further improvement of the efficiency of linear chiroptical response was achieved in the last decade by employing resonant metaphotonic structures made of plasmonic and dielectric materials.[12,13] In particular, very recently planar dielectric metastructures hosting photonic Mie resonances were shown to enhance the local chirality density and provide selective coupling to left-circularly polarized (LCP) and right-circularly polarized (RCP) waves.[14,15] This led to far-reaching implications for chiral emission,[16] chiral sensing,[17,18] characterization of quantum light,[19] and other areas.

Natural nonlinear optical activity is substantially more pronounced than linear chiroptical effects due to the high sensitivity of optical harmonics generated by chiral light to the molecular and structural asymmetry.[20] Such high sensitivity attracted special interest in nonlinear chiroptical effects, such as second- and third-harmonic CD, and led to comprehensive theoretical studies and experimental analysis of nonlinear optical activity for bulk media and planar interfaces in 1990s and early 2000s.[21–23] A high

*Address all correspondence to Kirill Koshelev, kirill.koshelev@anu.edu.au; Yuri Kivshar, yuri.kivshar@anu.edu.au

†These authors contributed equally to the paper.

increase of nonlinear optical activity was demonstrated for supramolecular arrays in helicene films of chloroform.[24]

The nonlinear CD for the nth harmonic can be evaluated as $(I_{\text{RCP}}^{(n\omega)} - I_{\text{LCP}}^{(n\omega)})/(I_{\text{RCP}}^{(n\omega)} + I_{\text{LCP}}^{(n\omega)})$, where $I_{\text{RCP(LCP)}}^{(n\omega)}$ is the full or co-polarized power of the nth harmonic for RCP (LCP) excitation. We note that sometimes the definition of the nth harmonic non-linear CD includes a factor of n, e.g., for second-harmonic generation (SHG) CD it is multiplied by 2 so the CD values can vary from -2 to 2. Similar to linear effects, the enhancement of nonlinear chiroptical effects beyond the limit of natural material response can be achieved by engineering chirality at a macroscopic scale.[25–28] What is different from the linear regime is that strong nonlinear optical activity also requires the high efficiency of nonlinear conversion. For this reason, resonances of metaphotonic structures are expected to play a crucial role, as they were shown to improve the frequency conversion efficiency dramatically by virtue of electric and magnetic hot spots enhancing the light–matter interaction.[29,30]

In this paper, we overview the development and major advances in the field of nonlinear chiral metaphotonics focusing on resonances of light and matter and their effect on nonlinear optical activity in nanostructures and metasurfaces. We start from a brief description of different types of resonances that can be realized in meta-optics with plasmonic and dielectric chiral metastructures, varying from surface plasmon polaritons to optical bound states in the continuum (BICs). Next, we describe briefly the history of research on nonlinear chiral photonics starting from nonresonant planar plasmonic arrays with macroscopic chiral geometry and moving to resonant metasurfaces that shape the nonlinear chiroptical response by virtue of plasmonic resonances. We then discuss how the efficiency of nonlinear chiroptical response can be improved by employing dielectric Mie-resonant metasurfaces and nanoantennas, which sustain substantially higher damage thresholds and provide additional degrees of freedom via excitation of optically induced magnetic resonances. We discuss how collective resonances of dielectric metasurfaces with a large quality factor can be employed to achieve maximal nonlinear chirality. Throughout the paper, we deliberate the role of the microscopic and macroscopic symmetries, geometrical phases, and various resonant effects. Finally, we conclude with an outlook on several novel opportunities in this rapidly expanding research area.

2 Resonances in Metaphotonic Structures

Chiroptical properties of metaphotonic structures composed of isolated nanoparticles or their arrays in the form of photonic crystals and metasurfaces are defined by the meta-atom geometry, lattice arrangement, and material properties. Due to the subwavelength size of individual scatterers, the resonant wavelengths in materials are comparable with the meta-atom characteristic size, allowing control of the resonance properties via geometry. Here, we briefly overview the most typical resonances in plasmonic and dielectric metastructures, shown schematically in the central panel of Fig. 1 (with the images adopted from several papers[31–36]) to better outline the differences they can provide in terms of nonlinear optical activity.

The fundamental modes of subwavelength plasmonic nanostructures are associated with localized surface plasmon resonances (LSPRs) representing nonpropagating coherent excitations of the free electron density coupled to the radiation continuum.[37] The LSPR frequency depends on the plasma frequency of the material, the shape of a nanoparticle, and its size. For small particles, the LSPR lifetime is determined by the nonradiative decay due to the material absorption. With an increase in the volume, the radiative loss channel starts to dominate the mode lifetime. The typical quality factor (Q factor) of dipolar and quadrupolar LSPRs is in the range of 2 to 10. Plasmonic resonances in isolated nanoparticles could provide the local electric field enhancement up to several hundred due to a deep subwavelength mode volume. An example of the scanning electron microscopy (SEM) image of a silver nano-particle with a 100 nm lateral size hosting LSPR at 520 nm[31] is shown on the left in Fig. 1(a).

Ordered arrays of plasmonic nanoparticles can host collective lattice modes, which can be generally divided into two classes: localized surface lattice resonances (SLRs), also called lattice surface modes, and nonlocal guided-mode resonances (GMRs). The SLRs originate from the near- and far-field coupling of LSPs of individual meta-atoms via diffractive orders of the lattice.[38] Formation of SLRs leads to the suppression of radiative losses of single LSPRs and thus results in a relatively large Q factor of the lattice mode up to several hundred units. The resonant wavelength of SLRs depends on the lattice parameters, including period and mutual arrangement, as well as meta-atom material and geometry. The electromagnetic fields of SLRs are predominantly localized at the nanoparticle surfaces. An example of the SEM image of the plasmonic metasurface composed of a rectangular array of gold nanobars[32] and supporting SLR at about 900 nm with $Q = 11$ is shown in the middle of Fig. 1(a). The GMR-type lattice modes are formed when the plasmonic array is positioned on top of a waveguiding dielectric layer, and the diffractive coupling between individual LSPRs occurs via the waveguide modes of the slab. For GMRs, the near fields are localized both on the particle surface and inside the waveguiding layer.

Plasmonic BICs represent a special class of plasmonic lattice modes with the Q factor, which tends to infinity due to destructive interference of radiation of the constituent LSPRs in the far field. The BICs are associated with nonlocal bound lattice modes with frequencies lying in the radiation continuum.[30] Here, we imply that nonlocal resonances represent spatially extended modes with strong interaction between meta-atoms.[39] The formation of quasi-BICs with a finite yet large Q factor can be achieved by introducing an asymmetry of meta-atoms or extrinsic asymmetry via the experimental setup. The first observation of plasmonic BICs was reported only very recently,[33] and the SEM image of the corresponding plasmonic metasurface composed of a rectangular array of U-shaped particles is shown on the right of Fig. 1(a). The metasurface supports a high-Q plasmonic quasi-BIC in the mid-IR frequency range. Recently, it was shown[40] that plasmonic BICs are related to out-of-plane SLRs, and their Q factor can exceed 2000.

Dielectric resonant structures emerged recently as a new platform in metaphotonics that allows effective localization of light in a bulk of material and additional degrees of freedom through the generation of artificial magnetic response.[30] The main building block of dielectric metastructures is an isolated dielectric nanoparticle hosting geometric Mie resonances, also called Mie modes. The Mie resonance wavelengths are defined as fractions of the lateral size of the nanoparticle multiplied by its refractive index. For high-index nanoresonators, the Mie modes with large values of the Q factor of up to several dozen can be readily realized in the visible and near-infrared (near-IR)
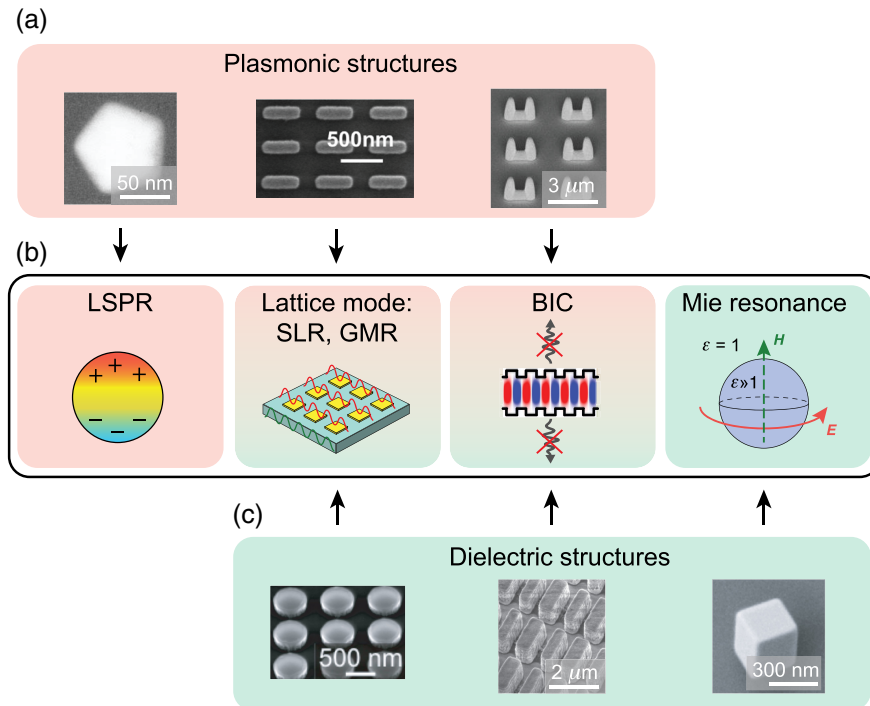
Fig. 1 Resonances in metaphotonic structures. (a) SEM images of selected plasmonic metastructures (red) with LSPR, SLR, and BIC resonances, respectively. (Left) Figure adapted from Ref. 31, with permission from AIP Publishing; (middle) adapted with permission from Ref. 32 ©2010, American Physical Society (APS); (right) adapted with permission from Ref. 33 ©2020 American Chemical Society (ACS). (b) Types of resonances in plasmonic (red), dielectric (green), and both types of materials (red-green). These include LSPR, lattice mode (SLR and GMR), BIC, and Mie resonance. (c) SEM images of selected dielectric metastructures with GMR, BIC, and Mie resonances. (Left) Figure adapted with permission from Ref. 34 ©2013 ACS; (middle) adapted with permission from Ref. 35 ©2022 ACS; (right) adapted with permission from Ref. 36 ©2020 ACS.

frequency ranges. Compared with metals,[41] high-index dielectric materials are free of material losses in the most relevant frequency ranges, which increases their potential for chiral nonlinear metaphotonics due to high damage thresholds. An example of an SEM image of a high-index dielectric nanocube composed of a lead-halide perovskite[36] supporting a high-order Mie mode at 535 nm with $Q = 15$ is shown on the right of Fig. 1(c).

Dielectric meta-atoms arranged in ordered arrays provide an additional way of control of chiroptical response via collective lattice modes. Similar to plasmonic lattices, dielectric metasurfaces, photonic crystal slabs, and membranes can host highly localized lattice Mie modes with weak near-field coupling and highly nonlocal GMRs with a large Q factor produced by strong diffractive coupling in the near and far field. In the case of GMRs, waveguiding can be realized, not in the substrate, but in the periodic array itself via collective oscillations of the polarization density. An example of an SEM image of a high-index dielectric metasurface composed of a square lattice of Si disks embedded in a low-index medium is shown on the left of Fig. 1(c). The metasurface supports almost degenerate magnetic and electric Mie lattice modes with the Q of order of 10 in the near-IR wavelength range.

The lattice modes of dielectric arrays can transform to high-Q photonic BICs and quasi-BICs under specific conditions, including unit cell asymmetry, parametric tuning, or mode strong

coupling.[30,42] The Q factor of the quasi-BIC mode can exceed 10^4 in broken-symmetry dielectric metasurfaces[43] and 10^5 in suspended membranes.[44] Chiral BICs can be realized in dielectric metasurfaces intrinsically, by using nonplanar meta-atoms with out-of-plane asymmetry,[14–16,45] or extrinsically, in planar metasurfaces with achiral meta-atoms with broken in-plane mirror symmetries placed on a substrate.[46] In addition to a high Q factor, BICs allow for advanced polarization control, provided they form topological vortices in the reciprocal space. An example of an SEM image of a high-index dielectric metasurface composed of a square lattice of Si bar dimers with different widths is shown in the middle of Fig. 1(c). The metasurface supports a quasi-BIC with $Q = 200$ in the mid-IR wavelength range.

In scattering, LSPR, Mie, lattice, and quasi-BIC resonances manifest normally themselves with a pronounced feature with an asymmetric Fano line shape due to interference with broad nonresonant modes and often termed generically as Fano resonances.[47] In particular, Fano resonances originating from quasi-BIC modes are sometimes referred to as high-Q or sharp Fano resonances.[29] Moreover, it can be shown that for quasi-BICs, the Fano asymmetry parameter is connected to the Q factor and diverges when the mode reaches its largest Q factor due to the strong mode coupling.[48] Also, quasi-BICs have been shown to govern the related effects of metamaterial-induced transparency and plasmonic-induced transparency.[42]

3 Nonlinear Chiral Plasmonic Metasurfaces

Next, we discuss the historical development of studies on nonlinear chiroptical metastructures, outlining several primary approaches allowing to achieve and control nonlinear optical activity. One of the first studies of chiral nonlinear response in nanostructured arrays was done in the early 2000s for non-resonant metallic metasurfaces. The limited fabrication quality of metallic nanostructures resulted in small nanoscale defects that provided a natural way of achieving 3D nonlinear optical activity.[49] The overall second-order response was shown to be related to a complicated interplay between plasmonic resonances of the particles and their structural defects. One of the pioneering works in this field[50] was devoted to the study of the second-order nonlinear characteristics of an array of L-shaped gold nanoparticles, shown in the SEM image in the upper panel of Fig. 2(a). The structure supported fundamental plasmonic resonances at 1020 nm for one linear polarization, and at 640 and 800 nm for the other polarization. Despite the presence of geometrical dichroism and resonances, the nonlinear response and activity were produced predominantly at the defects. The bottom panel of Fig. 2(a) shows the normalized second-harmonic (SH) signal for different orientations of the quarter-wave plate modifying the polarization of the incident beam from RCP to LCP and back. The signal was collected in the nonresonant regime at 1060 nm. The resulting SH efficiency was different for both circular polarizations, indicating a nonlinear SH-CD. The

defect contributions to the nonlinear optical response in such metasurfaces were later explained by effective higher multipolar terms in the nonlinear response.[53] This resulted in consequent studies on the separation of magnetic dipolar and electric quadrupolar effective nonlinear responses.[54,55] Finally, with the improvement of the sample quality, the dipole limit of the effective nonlinear chiroptical response was reached.[56]

Based on these developments, one of the key experimental methods to probe the nonlinear chirality of individual nanostructures with SHG microscopy was applied in a series of studies. In particular, in Ref. 51 the authors studied the nonlinear chiroptical response of metallic double-layer metasurfaces with a 3D chirality composed of gold twisted-cross nanodimers. The corresponding SEM images are shown in the top panel of Fig. 2(b). The meta-atoms can be left- or right-handed, depending on the mutual orientation of the crosses. The bottom panel of Fig. 2(b) shows the nonresonant SH microscopy images of the left-handed nanodimers for the LCP and RCP pump, respectively, at the pump wavelength of 1060 nm. The metasurface demonstrated the enhancement of SHG when the polarization of incident light coincided with the handedness of the nanostructure.

Early works in the field of nonlinear chirality in natural optical active crystals showed that the symmetry of the molecules defines the nonlinear optical activity via series of selection rules.[57] For bulk media, it was shown that harmonic generation for light with circular polarization follows the selection rule
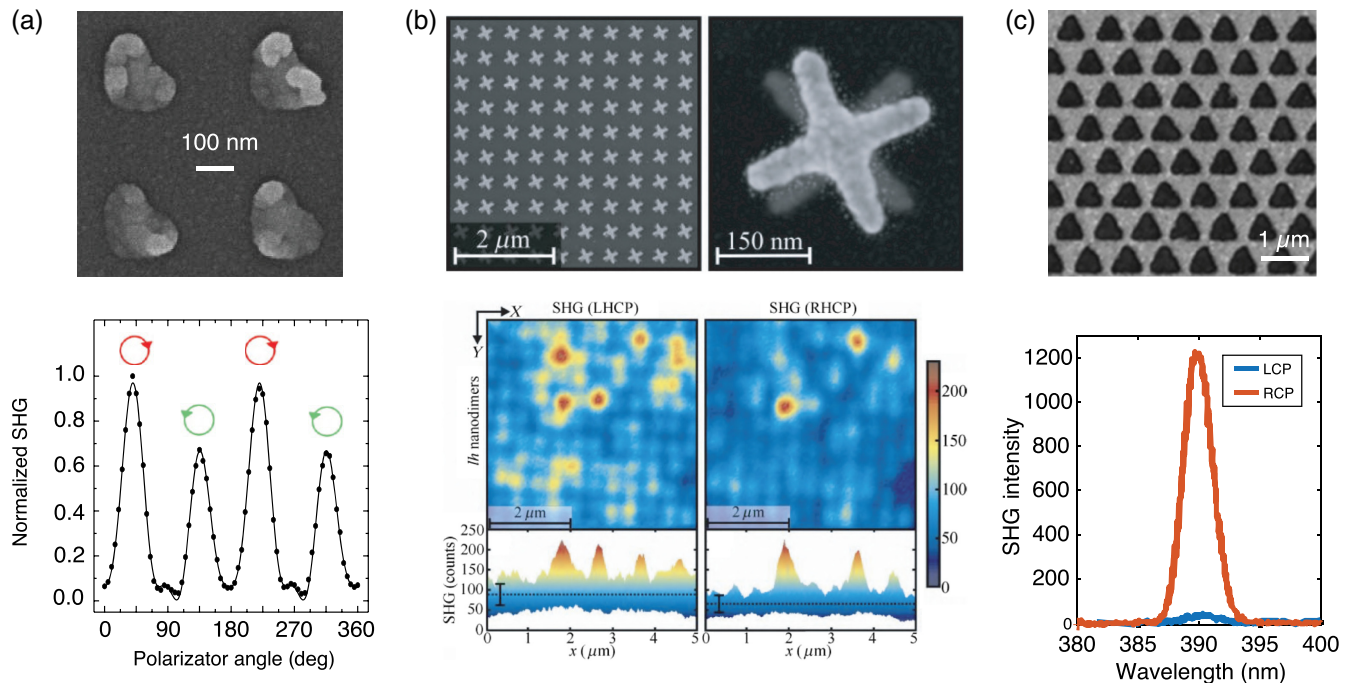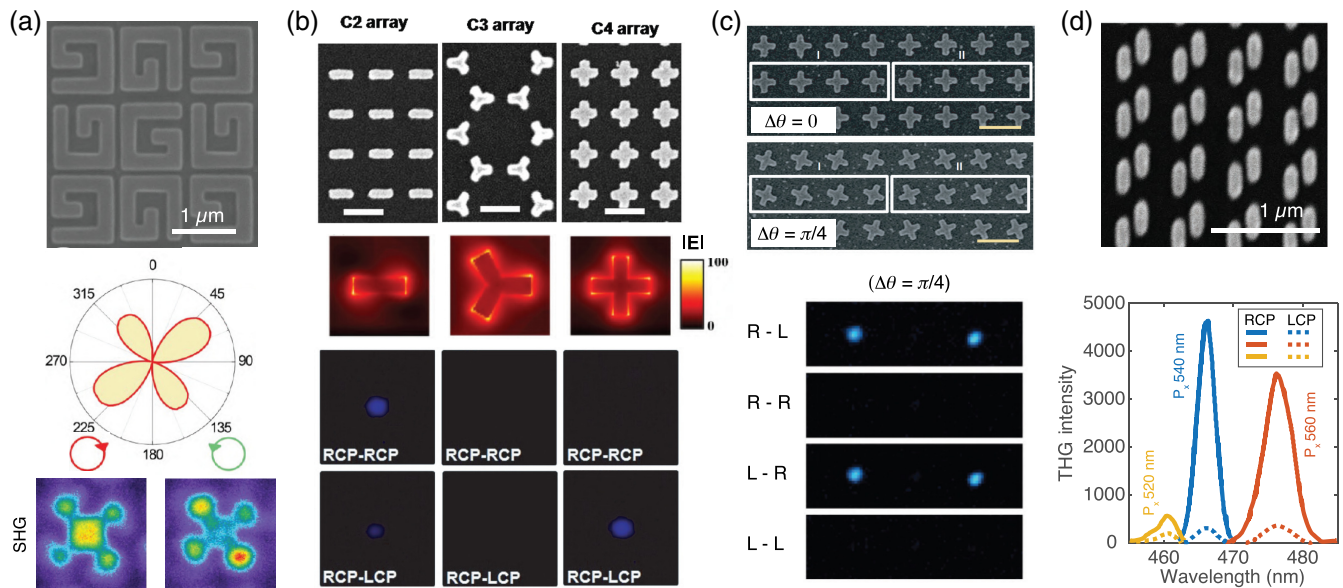

Fig. 2 Nonlinear chiroptical response from nonresonant metallic metastructures. (a) Metasurface composed of a square array of L-shaped gold nanoparticles with small defects. Figure adapted with permission from Ref. 50 ©2006 IOP Publishing (all rights reserved). Top: SEM image; bottom: nonresonant SH signal spectrum dependence on the orientation angle of the input beam polarizer. (b) Metasurface composed of gold twisted-cross nanodimers with 3D chirality. Figure adapted with permission from Ref. 51 ©2011 Optica. Top: SEM images; bottom: nonresonant SH microscopy maps for left-handed nanodimers for LCP and RCP pump, respectively. (c) Metasurface composed of triangular nanoholes in gold arranged in a honeycomb lattice. Top: SEM image; bottom: polarization-resolved SH spectra in the visible range for the LCP excitation. Figure adapted with permission from Ref. 52 ©2014 APS.

$Np_0 = ms + p_N$, where N is the order of harmonic generation, m is the order of rotational symmetry of the molecules, $p_0 = \pm 1$ and $p_N = \pm 1$ are the incident and harmonic wave handedness, respectively, and $s = 0, \pm 1, \ldots$ is an arbitrary integer.[58,59]

In early 2010s, these selection rules were generalized for macroscopic symmetry of metastructures outlining a key approach to control the chirality in metaphotonics. In particular, it was predicted that the selection rules can also be applied for harmonic generation in plasmonic metasurfaces composed of ordered meta-atom arrays with a specific lattice symmetry. For metallic nonresonant metasurfaces, this effect was first shown in a triangle hole-arrayed gold nanostructure,[52] the SEM image of which is shown in the top panel of Fig. 2(c). The selection rules for $N = 2$, $m = 3$ can be fulfilled only for $s = 1$ and $p_0 = -p_N$, which means that for a circularly polarized pump only a counter-polarized SH signal can be generated. The measured SH spectra of LCP and RCP components from this metasurface under the RCP excitation at 780 nm are shown in the bottom panel of Fig. 2(c). The nonlinear transmission measurements showed that the RCP pump generates a strong SH LCP signal with a very weak RCP component, which confirms the selection rules. This effect is also preserved for the opposite case, when the excitation beam is LCP. The weak nonzero co-polarized SH signal component arose only due to distortion of the shape from triangular geometry. For comparison,

cases of L-shaped and circular holes in a triangular lattice were studied. For L-shaped structures, the co-polarized SH component was as strong as the cross-polarized, while for circular holes the SH was zero, as it was prohibited by selection rules due to sixfold rotational symmetry.

One of the first works demonstrating nonlinear CD in resonant plasmonic metasurfaces was done in 2009 for a metasurface composed of gold G-shaped meta-atoms,[60] the SEM image of which is shown in the top panel of Fig. 3(a). The meta-atoms were arranged in a square lattice, with a supercell of four elements rotated by 90 deg with respect to the neighboring atom. By this, the metasurface was designed to possess a macroscopic rotational symmetry C_4 induced at the supercell level. The structures were pumped at 800 nm close to the LSPR resonance frequency. Change of the pump beam polarization with a quarter-wave plate caused the change in second-harmonic intensity, as shown in the bottom panel of Fig. 3(a), which resulted in the resonant SH-CD. The SHG microscopy images showed that the SH signal originated from the field hot spots attributed to plasmonic modes. This was the first work demonstrating that the arrangement of the nanostructures plays a crucial role, since upon reordering them, the SH-CD effect vanishes. Depending on the handedness of the nanostructures, the SHG sources exhibited a ratchet wheel pattern with a different sense of rotation. This allows for the possibility of optically determining the

Fig. 3 Nonlinear chiroptical response from resonant plasmonic metasurfaces. (a) Plasmonic metasurface with LSPR resonances composed of supercells of gold G-shaped meta-atoms arranged in a square lattice with C_4 rotational symmetry. Top: SEM image; bottom: SH signal dependence on the pump polarization and SH microscopy maps for LCP and RCP excitation. Figure adapted with permission from Ref. 60 ©2009 ACS. (b) Nonlinear metasurfaces supporting plasmonic lattice modes with engineered macroscopic C_2, C_3, and C_4 rotational symmetry. Top: SEM image; center: mode field profiles; bottom: TH signal maps for LCP and RCP excitation for corresponding metasurfaces. Figure adapted with permission from Ref. 61 ©2014 APS. (c) Nonlinear Pancharatnam–Berry phase metasurface composed of gold crosses hosting LSPR resonances in the near-IR range. Top: SEM image; bottom: experimental diffraction patterns of TH signals for the metasurfaces with geometric phase of 90 deg. Figure adapted with permission from Ref. 62 ©2015 Springer Nature. (d) Integrated nonlinear metasurface supporting hybrid plasmonic-photonic modes. Top: SEM image; bottom: TGH intensity for LCP and RCP excitation depending on the period of plasmonic metasurface P_x. Figure adapted with permission from Ref. 63 ©2019 John Wiley and Sons.

handedness of a material by observing it with one circularly polarized incident beam.

Later, it was shown that even pumped by linearly polarized light, the gold specially oriented G-shaped nanostructures demonstrate SH hot spots, whose arrangement is dependent on the handedness.[64] Another proposed method of chirality determination by linear light was based on SHG, depending on the rotation of the sample.[64] This was the first observation of a nonlinear chiroptical effect with magnetic dipoles. Later, it was shown that superchiral light is the local enhancement of the chirality density above the value for circularly polarized light in vacuum, and the SHG process is fundamentally linked via its dependence on the electric quadrupolar response of the resonant structures.[65] In addition, the study of CD in an optical SHG in planar symmetrical arrays of gold G-shaped nanostructures showed that nonlinear CD demonstrated a strong dependence of the value and the sign of the effect on the angle of incidence of the incident wave.[66]

The macroscopic selection rules for nonlinear chiroptical response of resonant plasmonic metasurfaces were first outlined in the work.[61] The SEM images of gold metasurfaces studied in the paper are shown in the top panel of Fig. 3(b). The geometry of meta-atoms and their arrangement were chosen to reproduce the rotational symmetry of the second, third, and fourth orders, respectively. The structures supported broad fundamental LSPRs at about 1300 nm, with the field profiles shown in the central panel of Fig. 3(b). The bottom panel of Fig. 3(b) shows experimentally measured THG images for different circular polarizations of pump and filtered harmonic polarization. The measurements confirm that selection rules applied to the lattice symmetry of the metasurface state that RCP or LCP harmonics can be generated only in two- and fourfold rotationally symmetric structures, but the chiral THG is forbidden for the threefold rotational symmetry configuration. It was also shown that this effect can be weakly disturbed at the microscopic level by the resonant contribution of modes, whose near field has out-of-plane noncircular polarization components. A separate study was devoted to the nonlinear chiroptical response of quasi-crystal resonant plasmonic metasurfaces. In the paper,[67] gold meta-atoms in nonlinear chiral metasurface arranged in a Penrose quasi-crystal were shown to demonstrate chiral SHG, which inverts circularly polarized pump from RCP to LCP and vice versa, similar to selection rules for regular photonic lattices.

One of the pioneering works demonstrating giant nonlinear optical activity in a plasmonic metasurface was done in 2012 for a metasurface composed of a square lattice of split-ring hole resonators.[68] The demonstrated resonant nonlinear optical activity was caused by direct two-photon absorption. This effect was shown to manifest itself via power-dependent circular birefringence and CD. The chirality was induced by breaking the symmetry extrinsically with an oblique incidence of the incident beam. A related observation of nonlinear SHG from achiral metasurfaces with broken in-plane symmetries was done later in 2016.[69] It was shown that intrinsic or extrinsic geometrical 3D chirality is not necessary for introducing strong CD for harmonic generations. Specifically, a near-unity CD for both SHG and THG attributed to nonlinear symmetry breaking was demonstrated for engineered resonant plasmonic metasurfaces with broken in-plane mirror symmetries. We note that compared to the SHG enhancement, the observed values of THG signal were relatively low.

Another prominent concept in nonlinear chiral metaphotonics is the Pancharatnam–Berry phase, applied for control of harmonic signal polarization and direction pumped by circular light.[70] The local effective nonlinear dipole moment $\mathbf{p}_m$ for an LCP or RCP pump incident along the rotational axis of a meta-atom can be expressed in the basis of circularly polarized waves as $\mathbf{p}_m(\varphi) = \alpha^{(m)}(\varphi)\mathbf{E}^m$. Here, φ is the angle of meta-atom rotation with respect to the primary lattice axes, $\alpha^{(m)}$ is the polarizability constant for the mth order nonlinear process, and $\mathbf{E}$ is the pump electric field with LCP or RCP polarization. The polarizability can be expressed as $\alpha^{(m)}(\varphi) \propto \exp[i(m \pm 1)\varphi]$ for the harmonic photons with cross- and co-polarization of the electric field, respectively. Thus, by controlling the geometrical orientation, it is possible to control the phase of the nonlinear signal and construct functional metasurfaces. One of the pioneering experimental demonstrations of the Pancharatnam–Berry metasurfaces was done for a gold plasmonic metasurface for continuous control of the nonlinearity phase for harmonic generation.[62] The SEM images of the studied structures are shown in the top panel of Fig. 3(c). The structures supported broad dipolar LSPR modes at about 1220 nm. Measured diffraction patterns of TH signals shown in the bottom panel of Fig. 3(c) for the metasurface with meta-atoms rotated by 90 deg demonstrated selective generation of ±1 diffraction orders. Later, using a similar concept, simultaneous control of spin and orbital angular momentum of SH signal in plasmonic metasurface was shown.[71] Later, this physics was generalized for non-dipolar responses of resonant phase metasurfaces.[72] More examples of Pancharatnam–Berry are discussed in the topical review in Ref. 26.

One of the essential drawbacks of plasmonic metasurfaces is their two-dimensional (2D) nature, which prevents them from exhibiting strong nonlinear optical activity. Recently, employing integrated plasmonic-dielectric structures supporting hybrid plasmonic-photonic modes was suggested.[63] The authors studied a plasmonic metasurface composed of a square lattice of gold nanodimers on top of a silicon-on-insulator wafer forming a waveguide; the SEM image is shown in the top panel of Fig. 3(d). The parameters of plasmonic lattice resonance were tuned by adjusting the metasurface geometry to couple it with the Fabry–Perot resonance of the waveguiding Si layer, which exhibited a broad dip in reflection at 1410 nm. The resulting hybrid mode exhibited a Q factor of about 100. The measured TH signal exhibited strong nonlinear CD, which also depended on the periodicity of the plasmonic metasurface, as shown in the bottom panel of Fig. 3(d). Another demonstration of a chiral nonlinear hybrid metasurface was done very recently for an Au–ZnO integrated nanostructure.[73] The structure was composed of nanoholes in gold arranged into a metasurface and covered with a ZnO dielectric layer. The hybrid metasurface demonstrated the enhancement of THG efficiency compared to a bare ZnO film and the possibility of multiplexed nonlinear holograms with four channels, which is based on the circular polarization of the fundamental excitation and hologram signal. Finally, we also mention another example of hybrid metasurfaces called polaritonic metasurfaces. Very recently, such polaritonic metasurfaces were demonstrated on a platform of resonant plasmonic metasurfaces integrated with a multiple semiconductor quantum well structure. They demonstrated resonant enhancement of second- and third-order susceptibilities due to intersubband transitions.[74] The structure was pumped in mid-IR range at about 10 μm wavelength and a combination of the strong nonlinear response of SH and TH signals and high nonlinear CD reaching values up to 1 was demonstrated.

4 Resonant Dielectric Metastructures

The plasmonic platform has several fundamental limitations hindering strong nonlinear chiroptical effects. The major ones are a low damage threshold, which is essential for high-intensity laser powers needed for nonlinear operation, and 2D geometry, which inherently prevents out-of-plane symmetry breaking required for strong optical activity. Hybrid platforms discussed in the previous section offer an intermediate solution; however, they are limited due to large footprint or similar problems with heating loss. Dielectric metasurfaces and nanostructures offer a favorable alternative to plasmonic nonlinear metasurfaces because of their robustness to absorption losses, and property to host geometrical resonances of a higher order that exploit the out-of-plane dimension, thus providing strong intrinsic linear and nonlinear chirality. In this section, we overview the recent progress in employing dielectric metastructures for enhancement and control of the nonlinear chiroptical response. The field is very young, and only a few demonstrations have been done so far. We start from dielectric periodic membranes and oligomers of individual nanoresonators hosting GMR and Mie modes, respectively.

The concept of engineering the nonlinear response via the macroscopic symmetry of the photonic structure, which we discussed for plasmonic metasurfaces, was recently transferred to dielectric periodic membranes.[75] The authors studied a vacuum ultraviolet (VUV) TH signal from a suspended dielectric γ-Al_2O_3 photonic crystal slab with circular air holes arranged in a square lattice so the structure formed a free-standing membrane; the schematic and SEM image are shown in the top and central panels of Fig. 4(a). The structure supported GMR modes in the visible range, manifesting themselves as dips in the transmission spectrum; see the central panel of Fig. 4(a). The measured VUV TH spectrum for the RCP excitation, shown in the bottom panel of Fig. 4(a), demonstrates the selection rule prohibiting co-polarized RCP THG for the fourfold lattice symmetry C_4. The nonzero RCP TH signal is attributed to deviations in the lattice shape transforming it to rectangular geometry. The measured VUV TH spectrum for the LCP excitation showed the opposite polarization of the harmonic signal with the same magnitude, confirming that the nonlinear TH CD is zero due to the in-plane mirror symmetries of the unit cell. In a very recent work, a VUV nonlinear metalens was demonstrated based on Pancharatnam–Berry phase concept.[78] The structure was composed of triangular ZnO meta-atoms on glass substrate supporting a magnetic dipole GMR mode. The lensing effect for the SH signal was achieved for circularly polarized excitation by arranging the meta-atoms with a certain Pancharatnam–Berry phase into a defined phase pattern. We note that the sufficient intensity of the VUV signal achieved in both papers was enabled by the high damage threshold of dielectric materials.

Recently, the first observation of the nonlinear optical activity of the SH hyper-Rayleigh scattering, that was predicted more than 40 years ago, was achieved with metallic helical structures suspended in solution.[79] Later, it was followed by consequent observation of the TH Rayleigh scattering for metallic helices.[80] Very recently, this concept was transferred to dielectric nanoparticles supporting vectorial Mie resonances, demonstrating strong TH CD in 3D chiral CdTe nanohelices,[76] with a schematic shown in the top panel of Fig. 4(b). The left- and right-handed nanohelices were fabricated by variation of the chemical synthesis method and suspended in solution. The structures

showed noticeable ellipticity in the linear scattering, which is in agreement with the calculated differential cross sections, as shown in the central panel of Fig. 4(b). The nanohelices generated the TH preserving the polarization of the circular fundamental beam regardless of the handedness. The magnitude of measured THG was different for the LCP and RCP excitation, depending on the input laser power; see the bottom panel of Fig. 4(b).

Very recently, the influence of relative atomic lattice orientation and macroscopic meta-molecule geometry on the nonlinear optical activity was studied experimentally. In the work,[77] it was shown that an AlGaAs nanodimer [see the top panel of Fig. 4(c)] hosting high-Q Mie resonances can provide strong SH CD for specific orientations of the particles with respect to each other. The SH CD was close to zero for a single particle but increased substantially for the dimer with specific relative crystal axes orientation, as shown in the central and bottom panels of Fig. 4(c). This work led to theoretical analysis of conditions for nonzero SH CD in individual nanoparticles and oligomers depending on the atomic lattice orientation and macroscopic symmetry of the metamolecule,[81] based on earlier knowledge of selection rulers for nonlinear processes in nanostructures of different shapes.[82,83]

Recent works also include theoretical analysis of intensity-dependent nonlinear chiroptical response driven by GMR modes in Si metasurfaces[84] and numerical study of chiral SHG in LN metasurfaces with Z-shaped meta-atoms in a square lattice on gold substrates.[85]

5 Metasurfaces with BICs

One of the most promising concepts for chiral nonlinear metaphotonics is associated with chiral quasi-BICs in dielectric resonant metasurfaces.[14,15] As outlined above, quasi-BICs were experimentally demonstrated to provide very strong field enhancement in the volume of nanostructures leading to the effective generation of optical harmonics, self-action effects, and high-harmonic generation.[35,86,87] The combination of chiral-BICs with the enhancement of nonlinear response provides a promising route for giant nonlinear optical activity.

The first theoretical concept of applying quasi-BICs in dielectric metasurfaces for enhancement of nonlinear CD was proposed by Gandolfi et al.[88] who considered a Si metasurface composed of asymmetric dimers placed on a glass substrate hosting quasi-BIC in the near-IR frequency range. The authors demonstrated numerically that such structures can achieve near-unity TH CD in the vicinity of the quasi-BIC mode together with the enhancement of the overall TH signal. This concept was later applied to double-layer photonic crystal slabs with asymmetric dimer-shaped holes in Si film.[89]

The pioneering experimental observations of chiral nonlinear BICs for strong nonlinear CD have been reported only recently.[46,90] Shi et al.[46] studied an Si metasurface composed of a square lattice of asymmetric meta-atoms, with the schematic and SEM images shown in the top and bottom left panels of Fig. 5(a). The in-plane asymmetry of the unit cell due to the parameter $\delta = W_2 - W_1$ induced transition from symmetry-protected BIC to quasi-BICs, which were observed in the near-IR range for both LCP and RCP polarizations; see the top right panel of Fig. 5(a). The linear CD reached the value of 0.65 at the resonance. The nonlinear measurements revealed that the TH intensity is increased dramatically at the quasi-BIC wavelength of 1390 nm for the RCP signal, contributing to a
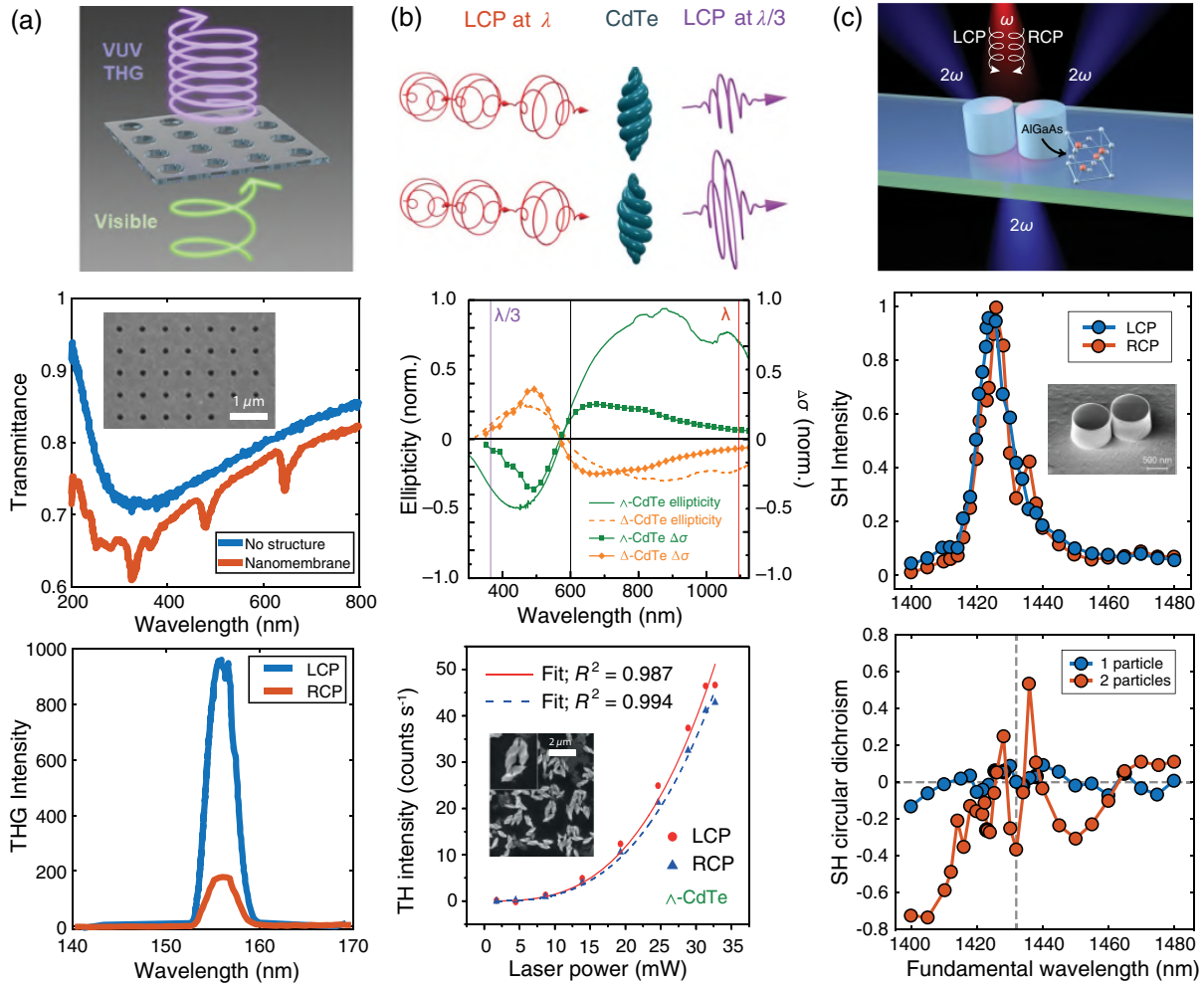
Fig. 4 Nonlinear chiroptical response from resonant dielectric metastructures. (a) VUV THG from dielectric γ-Al_2O_3 photonic crystal membrane hosting GMR modes. Top: schematic; center: linear transmission for structured and unstructured film and SEM image; bottom: LCP and RCP components of the TH intensity for the RCP pump beam. Figure adapted with permission from Ref. 75 ©2020 Optica. (b) TH CD from Mie-resonant CdTe nanostructured helices. Top: schematic; center: measured linear ellipticity and calculated differential extinction cross-section spectra; bottom: TH intensity in the forward direction versus pump laser power for the LCP and RCP pump and SEM image. Figure adapted with permission from Ref. 76 ©2022 Springer Nature. (c) Nonlinear CD in Mie-resonant dimer by breaking symmetry. Top: schematic; center and bottom: measured SH intensity and SH CD for LCP and RCP pump. Figure adapted with permission from Ref. 77 ©2021 ACS.

large TH CD of 0.93, as can be seen in the bottom right panel of Fig. 5(a).

Another paper[90] focused on the study of the impact of different kinds of high-Q optical resonances in dielectric metasurfaces on nonlinear optical activity, and maximization of the TH efficiency and TH CD simultaneously by virtue of quasi-BICs and other photonic resonances. The authors studied an Si metasurface composed of L-shaped asymmetric particles with the asymmetry defined as $dL = S_2 - S_1$; see the schematic and SEM image in the left panels of Fig. 5(b). The authors demonstrated that the metasurface hosts five quasi-BICs and one GMR mode in the range from 1250 to 1500 nm, for which the Q factor and wavelength can be gradually shifted by changing the asymmetry parameter dL from 100 to 300 nm. The TH signal was

maximized for specific values of dL in this range, different for each mode, which was explained by the critical coupling effect due to parasitic surface scattering losses, recently outlined for nonlinear quasi-BIC metasurfaces.[86,91] It was shown that the TH conversion efficiency can be maximized for both quasi-BICs and GMR mode reaching the same magnitude, which was attributed to the moderate fabrication quality of the metasurface. The co-polarized TH signals for the LCP and RCP excitation, respectively, measured for the optimized sample satisfying the critical coupling condition were shown to differ substantially in the vicinity of the BIC resonances, as shown in the top right panel of Fig. 5(b). It was observed experimentally that TH CD can be changed gradually by changing the asymmetry parameter dL from large negative to large positive values with keeping the
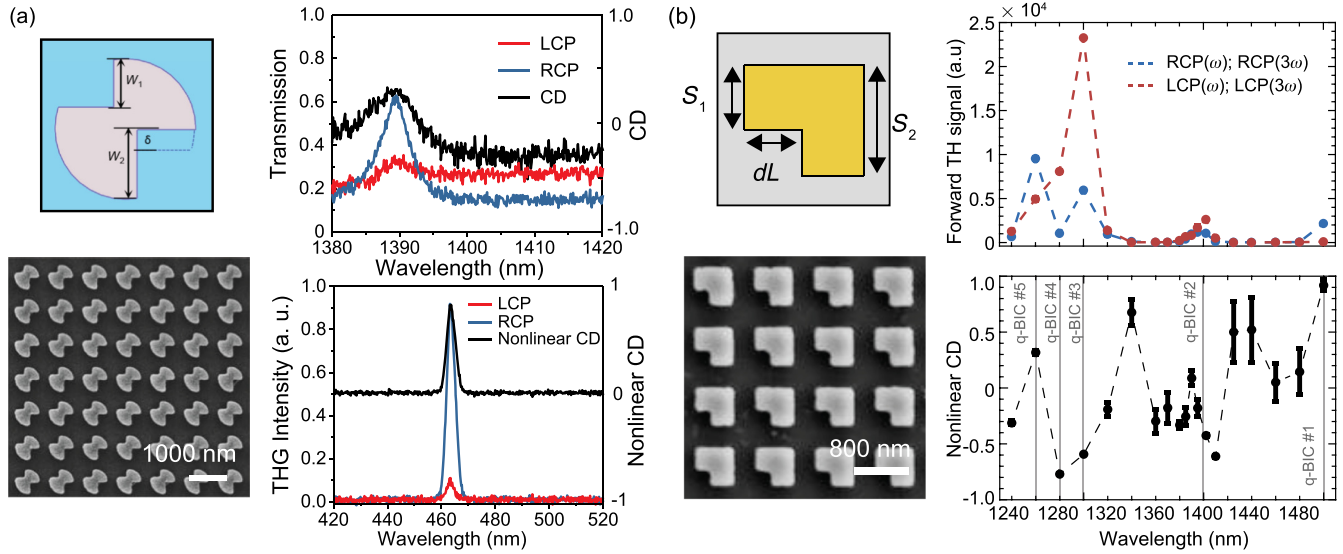
Fig. 5 Nonlinear chiral high-Q dielectric metasurfaces supporting quasi-BICs. (a) Chiral broken-symmetry nonlinear metasurface hosting a quasi-BIC mode. Left: schematic and SEM image; right: linear transmission and CD (upper) and TH intensity and TH CD (lower) for the LCP and RCP pump in the vicinity of the quasi-BIC resonance. Figure adapted with permission from Ref. 46 (CC-BY). (b) Asymmetric Si metasurface demonstrating record-high TH CD with strong THG efficiency via excitation of quasi-BICs and GMR mode. Left: schematic and SEM image; right: measured forward TH signal and TH CD for the optimized sample with d$L = 300$ nm. Figure adapted with permission from Ref. 90 ©2023 ACS.

TH intensity large. The maximal measured nonlinear TH CD reached the values of −0.771 and 0.918, which is the record-high demonstrated value for chiral dielectric metasurfaces, to the best of our knowledge. We notice that the high impact of nanofabrication defects on the quality of quasi-BIC resonances in dielectric metasurfaces was outlined in the recent work[92] and just very recently extended to the case of chiral quasi-BIC metasurfaces.[93]

6 Conclusion and Outlook

In recent years, we observe a rapid growth of the studied in chiral nonlinear metaphotonics due to refocusing of nanophotonics research from plasmonic to dielectric structures hosting versatile Mie and lattice resonances. We believe that several directions will attract attention in this field in the near future. Below, we mention briefly only some of those developments, including chiral generation of higher-order optical harmonics, chiral quantum optics, chiral polaritonics, chiral cavities, and topological photonics.

High-harmonic generation (HHG) from nanostructured solid materials was observed for the first time only a few years ago,[94] which led to increased attention to the generation of ultrafast pulses with resonant nanostructures made of dielectric and semiconductor materials, ranging from Si[35] and GaP[95] to halide perovskites.[96] We anticipate that the studies of chirality combined with HHG will be the next step in this direction, following the earlier observation of a bright, phase-matched, extreme UV circularly polarized high-harmonics source in gases.[97] Bridging high nonlinear CD with efficient HHG in nanophotonics could allow for extra control of ultrafast light–matter interaction in the extreme UV and soft X-ray frequency ranges. The recent work presented a theory of optical chirality for HHG in bulk nonlinear media uncovering the role of noninstantaneous polarization-associated chirality and time-scale-weighted polarization-associated chirality, and showing that these quantities link the chirality of multichromatic pumps and their generated attosecond pulses.[98]

Control of nonclassical light and enhancement of quantum nonlinear processes, such as spontaneous parametric downconversion (SPDC) with structured metasurfaces, is a hot topic recently emerging in metaphotonics.[99] The current active developments suggest new methods of control of quantum light, including measuring photon statistics, quantum entanglement, and detecting single photons. Several very recent studies explored the chiral properties of photons as a new avenue of quantum optics and photonics. Last year, dielectric metasurfaces pumped with circularly polarized light were used for characterization of the orbital angular momentum of quantum states in the SPDC process.[19] Another very recent study demonstrated optical spin–orbit interaction in the SPDC process realized through a nonlinear crystal with threefold rotational symmetry.[100] Following these studies, we foresee a variety of theoretical and experimental studies of chirality in quantum light interaction with metastructures empowered by optical resonances.

One of the very latest discoveries in chiral metaphotonics is the field of chiral polaritonics, describing formation of polaritons exhibiting chiral features via interaction between chiral quantum emitters and modes of chiral cavities.[101] This field is in its infancy, and the very first models have been developed to describe the behavior of chiral polaritons in the formalism of cavity quantum electrodynamics.[102] We believe that a variety of novel effects will be discovered soon in nonlinear chiral polaritonics that could be enabled by strong coupling between chiral light and nonlinear matter.

Using chiral metasurfaces, one can build very different optical cavities, depending on the desired functionality. More specifically, different pairs of metasurfaces can constitute chiral metacavities supporting counterpropagating waves of the same circular polarization. Such cavities based on chiral mirrors, possess remarkable excitation selectivity;[103] for example, the intensity of a helical standing wave excited by incident LCP waves is by more than 2 orders of magnitude higher than when being excited by RCP waves. Reciprocally, the Purcell factor of a right-handed chiral emitter inside such a cavity exceeds by more than an order of magnitude that of a left-handed emitter. Recently, a particular example of such a metacavity based on an aluminum mirror and a metasurface consisting of a square lattice of silicon triangular prisms was used to realize chiral electroluminescence from a plain perovskite layer.[104]

Finally, we wish to mention the emerging field of nonlinear topological photonics, which merges the physics of topological phases with nonlinear optics.[105] In topological systems, topological protection in the linear regime is associated with the topological edge states that occur in counterpropagating pairs with opposite spin. Nonlinearity may introduce asymmetry resulting in optical nonreciprocity, such as preferential lasing of a single-mode handedness or chirality.

Acknowledgments

References

1. L. D. Barron, *Molecular Light Scattering and Optical Activity*, Cambridge University Press (2009).
2. O. Kfir et al., "Nanoscale magnetic imaging using circularly polarized high-harmonic radiation," *Sci. Adv.* **3**(12), eaao4641 (2017).
3. B. Ranjbar and P. Gill, "Circular dichroism techniques: biomolecular and nanostructural analyses-a review," *Chem. Biol. Drug Des.* **74**(2), 101–120 (2009).
4. N. Berova, K. Nakanishi, and R. W. Woody, *Circular Dichroism: Principles and Applications*, John Wiley & Sons (2000).
5. J. Pendry, "A chiral route to negative refraction," *Science* **306**(5700), 1353–1355 (2004).
6. B. Wang et al., "Chiral metamaterials: simulations and experiments," *J. Opt. A: Pure Appl. Opt.* **11**(11), 114003 (2009).
7. S. S. Oh and O. Hess, "Chiral metamaterials: enhancement and control of optical activity and circular dichroism," *Nano Converg.* **2**, 24 (2015).
8. A. Papakostas et al., "Optical manifestations of planar chirality," *Phys. Rev. Lett.* **90**(10), 107404 (2003).
9. M. Kuwata-Gonokami et al., "Giant optical activity in quasi-two-dimensional planar nanostructures," *Phys. Rev. Lett.* **95**(22), 227401 (2005).
10. K. Konishi et al., "Observation of extraordinary optical activity in planar chiral photonic crystals," *Opt. Express* **16**(10), 7189–7196 (2008).
11. S. Volkov et al., "Optical activity in diffraction from a planar array of achiral nanoparticles," *Phys. Rev. A* **79**(4), 043819 (2009).
12. V. K. Valev et al., "Chirality and chiroptical effects in plasmonic nanostructures: fundamentals, recent progress, and outlook," *Adv. Mater.* **25**(18), 2517–2534 (2013).
13. M. Hentschel et al., "Chiral plasmonics," *Sci. Adv.* **3**(5), e1602735 (2017).
14. M. V. Gorkunov, A. A. Antonov, and Y. S. Kivshar, "Metasurfaces with maximum chirality empowered by bound states in the continuum," *Phys. Rev. Lett.* **125**(9), 093903 (2020).
15. A. Overvig, N. Yu, and A. Alù, "Chiral quasi-bound states in the continuum," *Phys. Rev. Lett.* **126**(7), 073001 (2021).
16. X. Zhang et al., "Chiral emission from resonant metasurfaces," *Science* **377**(6611), 1215–1218 (2022).
17. E. Mohammadi et al., "Nanophotonic platforms for enhanced chiral sensing," *ACS Photonics* **5**(7), 2669–2675 (2018).
18. M. L. Solomon et al., "Enantiospecific optical enhancement of chiral sensing and separation with dielectric metasurfaces," *ACS Photonics* **6**(1), 43–49 (2018).
19. M. Wang et al., "Characterization of orbital angular momentum quantum states empowered by metasurfaces," *Nano Lett.* **23**(9), 3921–3928 (2023).
20. T. Verbiest, M. Kauranen, and A. Persoons, "Light-polarization-induced optical activity," *Phys. Rev. Lett.* **82**(18), 3601–3604 (1999).
21. T. Petralli-Mallow et al., "Circular dichroism spectroscopy at interfaces: a surface second harmonic generation study," *J. Phys. Chem.* **97**(7), 1383–1388 (1993).
22. J. Byers, H. Yee, and J. Hicks, "A second harmonic generation analog of optical rotatory dispersion for the study of chiral monolayers," *J. Chem. Phys.* **101**(7), 6233–6241 (1994).
23. J. J. Maki, M. Kauranen, and A. Persoons, "Surface second-harmonic generation from chiral materials," *Phys. Rev. B* **51**(3), 1425–1434 (1995).
24. T. Verbiest et al., "Strong enhancement of nonlinear optical properties through supramolecular chirality," *Science* **282**(5390), 913–915 (1998).
25. L. M. Haupert and G. J. Simpson, "Chirality in nonlinear optics," *Annu. Rev. Phys. Chem.* **60**, 345–365 (2009).
26. G. Li, S. Zhang, and T. Zentgraf, "Nonlinear photonic metasurfaces," *Nat. Rev. Mater.* **2**(5), 17010 (2017).
27. K. Konishi, T. Kan, and M. Kuwata-Gonokami, "Tunable and nonlinear metamaterials for controlling circular polarization," *J. Appl. Phys.* **127**(23), 230902 (2020).
28. S. P. Rodrigues et al., "Review of optically active and nonlinear chiral metamaterials," *J. Nanophotonics* **16**(2), 020901 (2022).
29. B. Luk'yanchuk et al., "The Fano resonance in plasmonic nanostructures and metamaterials," *Nat. Mater.* **9**(9), 707–715 (2010).
30. K. Koshelev and Y. Kivshar, "Dielectric resonant metaphotonics," *ACS Photonics* **8**(1), 102–112 (2020).
31. J. Mock et al., "Shape effects in plasmon resonance of individual colloidal silver nanoparticles," *J. Chem. Phys.* **116**(15), 6755–6759 (2002).
32. V. Giannini, G. Vecchi, and J. G. Rivas, "Lighting up multipolar surface plasmon polaritons by collective resonances in arrays of nanoantennas," *Phys. Rev. Lett.* **105**(26), 266801 (2010).
33. Y. Liang et al., "Bound states in the continuum in anisotropic plasmonic metasurfaces," *Nano Lett.* **20**(9), 6351–6356 (2020).
34. I. Staude et al., "Tailoring directional scattering through magnetic and electric resonances in subwavelength silicon nanodisks," *ACS Nano* **7**(9), 7824–7832 (2013).
35. G. Zograf et al., "High-harmonic generation from resonant dielectric metasurfaces empowered by bound states in the continuum," *ACS Photonics* **9**(2), 567–574 (2022).
36. E. Tiguntseva et al., "Room-temperature lasing from Mie-resonant nonplasmonic nanoparticles," *ACS Nano* **14**(7), 8149–8156 (2020).

37. S. A. Maier, *Plasmonics: Fundamentals and Applications*, Springer (2007).
38. V. G. Kravets et al., "Plasmonic surface lattice resonances: a review of properties and applications," *Chem. Rev.* **118**(12), 5912–5951 (2018).
39. A. Overvig and A. Alù, "Diffractive nonlocal metasurfaces," *Laser Photonics Rev.* **16**(8), 2100633 (2022).
40. M. S. Bin-Alam et al., "Ultra-high-q resonances in plasmonic metasurfaces," *Nat. Commun.* **12**(1), 974 (2021).
41. C. Kern, M. Zürch, and C. Spielmann, "Limitations of extreme nonlinear ultrafast nanophotonics," *Nanophotonics* **4**(3), 303–323 (2015).
42. K. Koshelev et al., "Asymmetric metasurfaces with high-Q resonances governed by bound states in the continuum," *Phys. Rev. Lett.* **121**(19), 193903 (2018).
43. Z. Liu et al., "High-Q quasibound states in the continuum for nonlinear metasurfaces," *Phys. Rev. Lett.* **123**(25), 253901 (2019).
44. J. Jin et al., "Topologically enabled ultrahigh-Q guided resonances robust to out-of-plane scattering," *Nature* **574**(7779), 501–504 (2019).
45. Y. Chen et al., "Observation of intrinsic chiral bound states in the continuum," *Nature* **613**(7944), 474–478 (2023).
46. T. Shi et al., "Planar chiral metasurfaces with maximal and tunable chiroptical response driven by bound states in the continuum," *Nat. Commun.* **13**(1), 4111 (2022).
47. M. F. Limonov et al., "Fano resonances in photonics," *Nat. Photonics* **11**(9), 543–554 (2017).
48. E. Melik-Gaykazyan et al., "From Fano to quasi-BIC resonances in individual dielectric nanoantennas," *Nano Lett.* **21**(4), 1765–1771 (2021).
49. B. K. Canfield et al., "Chirality arising from small defects in gold nanoparticle arrays," *Opt. Express* **14**(2), 950–955 (2006).
50. B. K. Canfield et al., "A macroscopic formalism to describe the second-order nonlinear optical response of nanostructures," *J. Opt. A: Pure Appl. Opt.* **8**(4), S278 (2006).
51. M. J. Huttunen et al., "Nonlinear chiral imaging of subwavelength-sized twisted-cross gold nanodimers," *Opt. Mater. Express* **1**(1), 46–56 (2011).
52. K. Konishi et al., "Polarization-controlled circular second-harmonic generation from metal hole arrays with threefold rotational symmetry," *Phys. Rev. Lett.* **112**(13), 135502 (2014).
53. S. Kujala et al., "Multipole interference in the second-harmonic optical radiation from gold nanoparticles," *Phys. Rev. Lett.* **98**(16), 167403 (2007).
54. S. Kujala et al., "Multipolar analysis of second-harmonic radiation from gold nanoparticles," *Opt. Express* **16**(22), 17196–17208 (2008).
55. M. Zdanowicz et al., "Effective medium multipolar tensor analysis of second-harmonic generation from metal nanoparticles," *New J. Phys.* **13**(2), 023025 (2011).
56. R. Czaplicki et al., "Dipole limit in second-harmonic generation from arrays of gold nanoparticles," *Opt. Express* **19**(27), 26866–26871 (2011).
57. H. Simon and N. Bloembergen, "Second-harmonic light generation in crystals with natural optical activity," *Phys. Rev.* **171**(3), 1104 (1968).
58. O. E. Alon, V. Averbukh, and N. Moiseyev, "Selection rules for the high harmonic generation spectra," *Phys. Rev. Lett.* **80**(17), 3743–3746 (1998).
59. T. Higuchi et al., "Selection rules for light-induced magnetization of a crystal with threefold symmetry: the case of antiferromagnetic NiO," *Phys. Rev. Lett.* **106**(4), 047401 (2011).
60. V. K. Valev et al., "Plasmonic ratchet wheels: switching circular dichroism by arranging chiral nanostructures," *Nano Lett.* **9**(11), 3945–3948 (2009).
61. S. Chen et al., "Symmetry-selective third-harmonic generation from plasmonic metacrystals," *Phys. Rev. Lett.* **113**(3), 033901 (2014).
62. G. Li et al., "Continuous control of the nonlinearity phase for harmonic generations," *Nat. Mater.* **14**(6), 607–612 (2015).
63. F. Wang and H. Harutyunyan, "Observation of a giant nonlinear chiro-optical response in planar plasmonic–photonic metasurfaces," *Adv. Opt. Mater.* **7**(19), 1900744 (2019).
64. V. Valev et al., "Asymmetric optical second-harmonic generation from chiral G-shaped gold nanostructures," *Phys. Rev. Lett.* **104**(12), 127401 (2010).
65. V. K. Valev et al., "Nonlinear superchiral meta-surfaces: tuning chirality and disentangling non-reciprocity at the nanoscale," *Adv. Mater.* **26**(24), 4074–4081 (2014).
66. E. Mamonov et al., "Anisotropy versus circular dichroism in second harmonic generation from fourfold symmetric arrays of G-shaped nanostructures," *Phys. Rev. B* **89**(12), 121113 (2014).
67. Y. Tang et al., "Quasicrystal photonic metasurfaces for radiation controlling of second harmonic generation," *Adv. Mater.* **31**(23), 1901188 (2019).
68. M. Ren et al., "Giant nonlinear optical activity in a plasmonic metamaterial," *Nat. Commun.* **3**(1), 833 (2012).
69. S. Chen et al., "Giant nonlinear optical activity of achiral origin in planar metasurfaces with quadratic and cubic nonlinearities," *Adv. Mater.* **28**(15), 2992–2999 (2016).
70. M. Tymchenko et al., "Gradient nonlinear Pancharatnam-Berry metasurfaces," *Phys. Rev. Lett.* **115**(20), 207403 (2015).
71. G. Li et al., "Nonlinear metasurface for simultaneous control of spin and orbital angular momentum in second harmonic generation," *Nano Lett.* **17**(12), 7974–7979 (2017).
72. S. D. Gennaro et al., "Nonlinear Pancharatnam–Berry phase metasurfaces beyond the dipole approximation," *ACS Photonics* **6**(9), 2335–2341 (2019).
73. X. Hong et al., "Chiral third-harmonic metasurface for multiplexed holograms," *Nano Lett.* **22**(22), 8860–8866 (2022).
74. D. Kim et al., "Giant nonlinear circular dichroism from intersubband polaritonic metasurfaces," *Nano Lett.* **20**(11), 8032–8039 (2020).
75. K. Konishi et al., "Circularly polarized vacuum ultraviolet coherent light generation using a square lattice photonic crystal nanomembrane," *Optica* **7**(8), 855–863 (2020).
76. L. Ohnoutek et al., "Third-harmonic Mie scattering from semiconductor nanohelices," *Nat. Photonics* **16**(2), 126–133 (2022).
77. K. Frizyuk et al., "Nonlinear circular dichroism in Mie-resonant nanoparticle dimers," *Nano Lett.* **21**(10), 4381–4387 (2021).
78. M. L. Tseng et al., "Vacuum ultraviolet nonlinear metalens," *Sci. Adv.* **8**(16), eabn5644 (2022).
79. J. Collins et al., "First observation of optical activity in hyper-Rayleigh scattering," *Phys. Rev. X* **9**(1), 011024 (2019).
80. L. Ohnoutek et al., "Optical activity in third-harmonic Rayleigh scattering: a new route for measuring chirality," *Laser Photonics Rev.* **15**(11), 2100235 (2021).
81. A. Nikitina, A. Nikolaeva, and K. Frizyuk, "Nonlinear circular dichroism in achiral dielectric nanoparticles," *Phys. Rev. B* **107**(4), L041405 (2023).
82. M. Finazzi et al., "Selection rules for second-harmonic generation in nanoparticles," *Phys. Rev. B* **76**(12), 125414 (2007).
83. K. Frizyuk et al., "Second-harmonic generation in Mie-resonant dielectric nanoparticles made of noncentrosymmetric materials," *Phys. Rev. B* **99**(7), 075425 (2019).
84. L. Kang, Y. Wu, and D. H. Werner, "Nonlinear chiral metasurfaces based on the optical Kerr effect," *Adv. Opt. Mater.* **11**(10), 2202658 (2023).
85. K.-H. Kim and J.-R. Kim, "Dielectric chiral metasurfaces for second-harmonic generation with strong circular dichroism," *Ann. Phys.* **532**(8), 2000078 (2020).
86. K. Koshelev et al., "Nonlinear metasurfaces governed by bound states in the continuum," *ACS Photonics* **6**(7), 1639–1644 (2019).

87. I. S. Sinev et al., "Observation of ultrafast self-action effects in quasi-BIC resonant metasurfaces," *Nano Lett.* **21**(20), 8848–8855 (2021).

88. M. Gandolfi et al., "Near-unity third-harmonic circular dichroism driven by a quasibound state in the continuum in asymmetric silicon metasurfaces," *Phys. Rev. A* **104**(2), 023524 (2021).

89. Q.-S. Liu et al., "Dual-band chiral nonlinear metasurface supported by quasibound states in the continuum," *Ann. Phys.* **534**(12), 2200263 (2022).

90. K. Koshelev et al., "Resonant chiral effects in nonlinear dielectric metasurfaces," *ACS Photonics* **10**(1), 298–306 (2023).

91. N. Bernhardt et al., "Quasi-BIC resonant enhancement of second-harmonic generation in WS_2 monolayers," *Nano Lett.* **20**(7), 5309–5314 (2020).

92. J. Kühne et al., "Fabrication robustness in BIC metasurfaces," *Nanophotonics* **10**(17), 4305–4312 (2021).

93. L. Fagiani et al., "Modelling and nanofabrication of chiral dielectric metasurfaces," *Micro Nano Eng.* **19**, 100187 (2023).

94. G. Vampa et al., "Plasmon-enhanced high-harmonic generation from silicon," *Nat. Phys.* **13**(7), 659–662 (2017).

95. M. R. Shcherbakov et al., "Generation of even and odd high harmonics in resonant metasurfaces using single and multiple ultra-intense laser pulses," *Nat. Commun.* **12**(1), 4185 (2021).

96. P. Tonkaev et al., "Observation of enhanced generation of a fifth harmonic from halide perovskite nonlocal metasurfaces," *ACS Photonics* **10**(5), 1367–1375 (2023).

97. O. Kfir et al., "Generation of bright phase-matched circularly-polarized extreme ultraviolet high harmonics," *Nat. Photonics* **9**(2), 99–105 (2015).

98. O. Neufeld and O. Cohen, "Optical chirality in nonlinear optics: application to high harmonic generation," *Phys. Rev. Lett.* **120**(13), 133206 (2018).

99. A. S. Solntsev, G. S. Agarwal, and Y. S. Kivshar, "Metasurfaces for quantum photonics," *Nat. Photonics* **15**(5), 327–336 (2021).

100. Y. Wu et al., "Optical spin–orbit interaction in spontaneous parametric downconversion," *Optica* **10**(5), 538–543 (2023).

101. D. G. Baranov, C. Schäfer, and M. V. Gorkunov, "Toward molecular chiral polaritons," *ACS Photonics* **10**(8), 2440–2455 (2023).

102. M. Schäferling, "Chiral nanophotonics," *Springer Ser. Opt. Sci.* **205**, 159 (2017).

103. K. Voronin et al., "Single-handedness chiral optical cavities," *ACS Photonics* **9**, 2652–2659 (2022).

104. S. Kim et al., "Chiral electroluminescence from thin-film perovskite metacavities," *Sci. Adv.* **9**, eadh0414 (2023).

105. D. Smirnova et al., "Nonlinear topological photonics," *Appl. Phys. Rev.* **7**, 021306 (2020).

Kirill Koshelev received his PhD from the Australian National University in 2022. He is currently a postdoctoral fellow at the Department of Fundamental and Theoretical Physics of the Australian National University. His current research interests include theoretical and numerical approaches in dielectric metaphotonics, resonant nano-optics, and physics of non-Hermitian systems.

Pavel Tonkaev received his MS degree in physics from the ITMO University, Russia, in 2019. He is currently a PhD student under the supervision of Prof. Yuri Kivshar at the Australian National University. His research interests are in the fields of nanophotonics, metamaterials, and nonlinear physics.

Yuri Kivshar received his PhD in 1984 from Kharkov in Ukraine. During next few years, he worked at several research centers in the USA and Europe, and in 1993 he moved to Australia, where currently he is distinguished professor at the Australian National University. His research interests include nonlinear physics, metamaterials, and nanophotonics.